SINTEF
PROCEEDINGS
2

Proceedings of the 12th International Conference on Computational Fluid Dynamics in the Oil & Gas, Metallurgical and Process Industries

Progress in Applied CFD – CFD2017

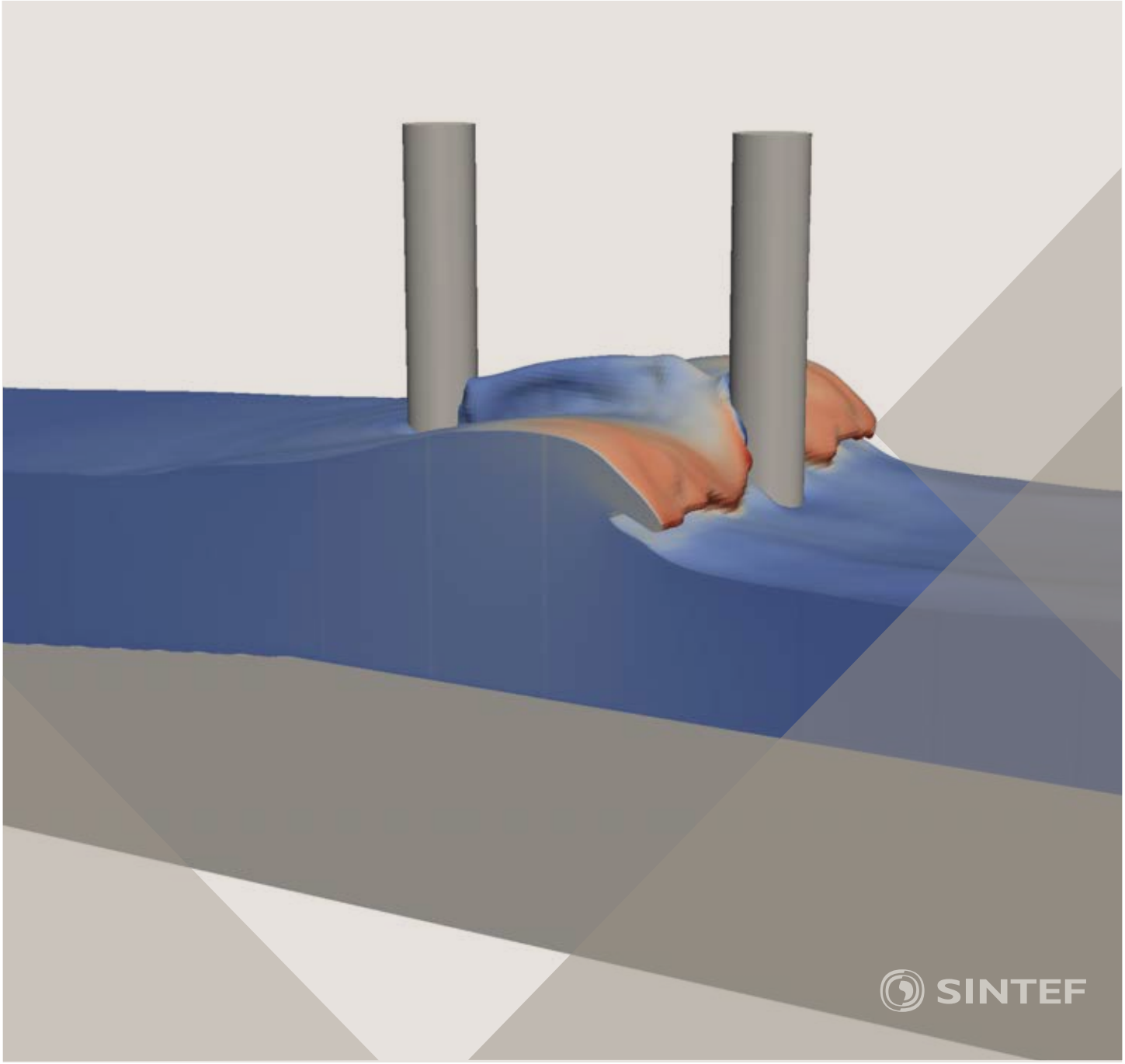

SINTEF

SINTEF Proceedings

Editors:
Jan Erik Olsen and Stein Tore Johansen

Progress in Applied CFD – CFD2017

Proceedings of the 12th International Conference on Computational Fluid Dynamics in the Oil & Gas, Metallurgical and Process Industries

SINTEF Academic Press

SINTEF Proceedings no 2
Editors: Jan Erik Olsen and Stein Tore Johansen
Progress in Applied CFD – CFD2017
Selected papers from 10th International Conference on Computational Fluid Dynamics in the Oil & Gas, Metallurgical and Process Industries

Key words:
CFD, Flow, Modelling

Cover, illustration: Arun Kamath

ISSN 2387-4295 (online)
ISBN 978-82-536-1544-8 (pdf)

SINTEF Academic Press
Address: Forskningsveien 3 B
PO Box 124 Blindern
N-0314 OSLO
Tel: +47 73 59 30 00
Fax: +47 22 96 55 08

www.sintef.no/byggforsk
www.sintefbok.no

SINTEF Proceedings
SINTEF Proceedings is a serial publication for peer-reviewed conference proceedings on a variety of scientific topics.
The processes of peer-reviewing of papers published in SINTEF Proceedings are administered by the conference organizers and proceedings editors. Detailed procedures will vary according to custom and practice in each scientific community.

PREFACE

This book contains all manuscripts approved by the reviewers and the organizing committee of the 12th International Conference on Computational Fluid Dynamics in the Oil & Gas, Metallurgical and Process Industries. The conference was hosted by SINTEF in Trondheim in May/June 2017 and is also known as CFD2017 for short. The conference series was initiated by CSIRO and Phil Schwarz in 1997. So far the conference has been alternating between CSIRO in Melbourne and SINTEF in Trondheim. The conferences focuses on the application of CFD in the oil and gas industries, metal production, mineral processing, power generation, chemicals and other process industries. In addition pragmatic modelling concepts and bio-mechanical applications have become an important part of the conference. The papers in this book demonstrate the current progress in applied CFD.

The conference papers undergo a review process involving two experts. Only papers accepted by the reviewers are included in the proceedings. 108 contributions were presented at the conference together with six keynote presentations. A majority of these contributions are presented by their manuscript in this collection (a few were granted to present without an accompanying manuscript).

The organizing committee would like to thank everyone who has helped with review of manuscripts, all those who helped to promote the conference and all authors who have submitted scientific contributions. We are also grateful for the support from the conference sponsors: ANSYS, SFI Metal Production and NanoSim.

Stein Tore Johansen & Jan Erik Olsen

Organizing committee:

Conference chairman: Prof. Stein Tore Johansen
Conference coordinator: Dr. Jan Erik Olsen
Dr. Bernhard Müller
Dr.Sigrid Karstad Dahl
Dr.Shahriar Amini
Dr.Ernst Meese
Dr.Josip Zoric
Dr.Jannike Solsvik
Dr.Peter Witt

Scientific committee:

Stein Tore Johansen, SINTEF/NTNU
Bernhard Müller, NTNU
Phil Schwarz, CSIRO
Akio Tomiyama, Kobe University
Hans Kuipers, Eindhoven University of Technology
Jinghai Li, Chinese Academy of Science
Markus Braun, Ansys
Simon Lo, CD-adapco
Patrick Segers, Universiteit Gent
Jiyuan Tu, RMIT
Jos Derksen, University of Aberdeen
Dmitry Eskin, Schlumberger-Doll Research
Pär Jönsson, KTH
Stefan Pirker, Johannes Kepler University
Josip Zoric, SINTEF

CONTENTS

OSCILLATORY FLOW AND MASS TRANSPORT IN A CORONARY ARTERY

Sargon A. GABRIEL[1*], **Yan DING**[1], **John A. GEAR**[1], **Yuqing FENG**[2†]
[1]Mathematics, School of Science, RMIT University, Melbourne, Victoria 3001, AUSTRALIA
[2]Mineral Resources, CSIRO, Clayton South, Victoria 3169, AUSTRALIA

[*] E-mail: sargon.gabriel@rmit.edu.au
[†] E-mail: yuqing.feng@csiro.au

ABSTRACT

Pulsatile flow is intrinsic to the cardiovascular system and is driven by the rhythmic beating of the heart. As a system for mass transport, the cardiovascular system hosts a variety of biochemical and cellular species whose transport is subjected to the corresponding flow oscillations. The influence is most prevalent near the heart and particularly within arteries, where pressure fluctuations are most significant. This makes modelling of long-term mass transport difficult to evaluate, since intermediate oscillations need to be explicitly resolved. By applying Reynolds averaging to the governing flow and mass transport equations on a representative period of oscillation, this problem may be alleviated. However, doing so introduces extra terms akin to the Reynolds stresses in the flow equations as well as perturbed-flux terms in the mass transport equations. These terms are investigated in the present study and their distributions assessed. A human right coronary artery is used as the subject geometry, wherein the oscillatory transport behaviour of blood flow and low density lipoprotein is studied.

Keywords: coronary artery, oscillation, period-average, pulsatile flow, species transport.

NOMENCLATURE

Greek Symbols

∂	partial derivative
δ_{ij}	Kronecker delta tensor
μ	dynamic viscosity, $[\mathrm{kg/m/s}]$
ρ	density, $[\mathrm{kg/m^3}]$
τ_{ij}	viscous stress tensor, $[\mathrm{kg/m/s^2}]$
$\boldsymbol{\tau_w}$	wall shear stress vector, $[\mathrm{kg/m/s^2}]$
φ	arbitrary scalar field variable
Δ_{ij}	strain-rate tensor, $[1/\mathrm{s}]$
Γ	domain boundary
Ω	domain

Latin Symbols

c	normalised species concentration
d	diameter, $[\mathrm{m}]$
$\boldsymbol{n}$	surface normal vector
p	pressure, $[\mathrm{kg/m/s^2}]$
ps	pulsatile-state (period-averaged)
ss	steady-state
t	time, $[\mathrm{s}]$
$\boldsymbol{u}$	velocity vector, $[\mathrm{m/s}]$
$\boldsymbol{x}$	spatial position vector, $[\mathrm{m}]$
C	species concentration
D	species diffusivity, $[\mathrm{m^2/s}]$
J	flux into a boundary
Pe	Péclet
Re	Reynolds

Sub/superscripts

0	reference condition (at the inflow)
i, j	Cartesian tensor indices[1]
F	fluid
I	inflow
O	outflow
W	wall

INTRODUCTION

The cardiovascular system is a circulatory transport system for blood that carries erythrocytes, thrombocytes, lipoproteins and other species throughout the body. The flow of blood within the cardiovascular system is driven by pressure differentials generated at the heart. As the heart periodically contracts and relaxes, the pressure differentials fluctuate, causing blood flow to oscillate about a non-zero net-period flow-rate. Correspondingly, the transport of blood-borne species is inherently oscillatory[2], with oscillations imparted by the advecting blood medium. Advective transport by blood flow is one of two dominant transport processes governing species within the cardiovascular system, with the other being diffusive transport. The net transport of a species may be therefore regarded as a competing balance between the two transport processes, with advection generally dominating within the bulk blood flow and diffusion near the vascular walls. This collective behaviour is quantified by the dimensionless Péclet number (Pe), which measures the respective rates of advective and diffusive transport.

At any point in the flow, advective transport is perceived almost equally amongst relatively passive blood-borne species (i. e. that do not significantly influence the flow field). However, diffusive transport can vary since diffusivity varies amongst species and hence, their corresponding Péclet numbers. A low Péclet number species (i.e. of high diffusivity

[1]The subscripts i, j are reserved for index notation of Cartesian tensors; all other subscripts are for designating variables and should not be interpreted as tensor indices. Repeated indices in a term imply Einstein summation notation. For the generic vector variable $\boldsymbol{\varphi}$, the element-wise absolute is designated by $|\varphi_i|$ and the Euclidean magnitude (2-norm) by $\|\boldsymbol{\varphi}\| = \sqrt{\varphi_i \varphi_i}$.

[2]The terms *oscillatory* and *pulsatile* are herein used interchangeably to describe the flow and are not differentiated with any distinct meaning.

within blood plasma), would be little influenced by the oscillatory flow and would conform to a near-regular transport. However, most blood-borne species are generally of high Péclet numbers in the bulk flow, such as low density lipoproteins (Pe $\sim 2\times10^8$) and oxygen (Pe $\sim 1\times10^6$) (Stangeby and Ethier, 2002). In such species, the dominance of advective transport implies a strong influence from the flow, and hence its oscillatory behaviour on their transport. From a modelling perspective, this presents a potential constraint for high Péclet number species transport, since the strong coupling to the flow in the bulk flow and increasing influence of diffusivity in the near-wall flow implies an interplay of varying length and time scales. That is, the corresponding response of the species to perturbations from the oscillating flow would spatially vary between the bulk and near-wall flow, requiring a large number of periods (i. e. computational time) to achieve a steady-periodic equilibrium state.

This is demonstrated in the transport of high Péclet number blood-borne species, in that whilst the flow may resolve to a steady-periodic regime within a reasonable ~ 5 periods of oscillation from resting-state initial conditions (Liu *et al.*, 2011), the same is not necessarily true for the species, which may take considerably longer (Sun *et al.*, 2007). This is especially problematic near vascular walls where other types of interactions may occur, such as transport into the walls and reactions with other species (Tarbell, 2003). For computational models of such species, this presents an inconvenience that may be infeasible to resolve within reasonable time and computational resources. Indeed, oscillatory flow and mass transport has been extensively investigated in past studies, such as those of Hong *et al.* (2012), Liu *et al.* (2011), Sakellarios *et al.* (2013) and Sun *et al.* (2007). However, the difficulty of attaining a steady-periodic regime still remains to be realised within feasible computational resources. In the objective of resolving this difficulty, the mechanics that influence the steady-periodic regime for flow and species transport are therefore investigated in the present study. Period-averaging techniques akin to those of turbulence modelling are applied to the governing flow and species transport equations, so that they may be compared to their equivalent steady-state conditions.

METHODOLOGY

A human right coronary artery (RCA) segment is selected as the subject geometry of study for this investigation. This is because coronary arteries are inherent with relatively small diameters and longitudinal variations in their geometry; the former is useful for reducing computational requirements as multiple periods of oscillation are to be computed, and the latter is useful for inducing variations in the distribution of near-wall species concentration. For this study, the species to be investigated is low density lipoprotein (LDL).

Geometry

The RCA geometry[3] to be investigated comprises of a single stem with no bifurcations or branches. The geometry comprises of the volumetric flow space (lumen) Ω_F, which is bounded by the wall Γ_W, inflow Γ_I and outflow Γ_O boundaries; see figure 1 (a). To ensure that the flow and species entering Ω_F are sufficiently developed from their boundary condition states, the inflow and outflow boundaries are extended by flow extensions of 5 [mm] and 10 [mm] respectively.

[3]Geometry provided by the Biofluid Mechanics Lab, Charité Universitätsmedizin Berlin.

The geometry is discretised using a longitudinally swept O-grid mesh that comprises of 2385 hexahedral elements per cross-section, which amounts to about 7.75×10^5 elements for the collective geometry; see figure 1 (b). For most of the volumetric flow space, the concentration of LDL is expected to be uniform, except near the wall where a thin mass transport boundary layer develops. The near-wall mesh is thus refined to sufficiently resolve the mass transport boundary layer, such that the first element layer height is about 2200 times smaller than the average inflow diameter d_I.

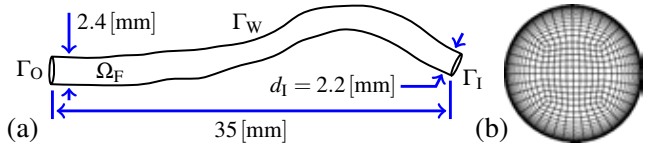

Figure 1: Detail of the RCA segment used for this study, with (a) geometry schematic (not including flow-extensions) and (b) cross-section O-grid mesh (coarsened for display).

Governing equations

To investigate the oscillatory behaviour of flow and mass transport of blood and blood-borne species, a continuum description is considered. That is, though it is recognised that blood comprises a heterogeneous suspension of particulates, the collective fluid is approximated as continuous on a sufficiently large macroscale level. For blood vessels with diameters significantly larger than that of an erythrocyte (i. e. red blood cell), the continuum fluid assumption is found to satisfactorily hold. However, special care needs to be made in resolving macroscale level properties such as rheology, which need to be described via constitutive models (Thiriet, 2008). For the present study, the arterial wall is assumed to be rigid and hence non-compliant. This assumption is made so that data processing of oscillatory blood flow and blood-borne species transport can be made within a fixed (i. e. Eulerian) reference frame. For example, the Eulerian reference frame allows for a spatially-invariant definition of period-averaging to be naturally realised. Otherwise, if the arterial wall is allowed to deform, then so would the volumetric flow space Ω_F. In such a case, special treatment would be required to define a spatially-invariant period-average within Ω_F.

Blood flow transport

To describe blood flow, the incompressible mass and momentum conservation (Navier–Stokes) equations are used. In conservative-form, these are respectively expressed by

$$\partial_i u_i = 0 \tag{1}$$

$$\rho\partial_t u_i + \partial_j\left(\rho u_i u_j - \tau_{ij} + p\delta_{ij}\right) = 0, \tag{2}$$

where u_i is a component of the blood's velocity field vector $\boldsymbol{u}$ and p is its scalar pressure field; δ_{ij} is the Kronecker delta. The viscous stress tensor is defined $\tau_{ij} = 2\mu\Delta_{ij}$ and the strain-rate tensor $\Delta_{ij} = \frac{1}{2}\left(\partial_i u_j + \partial_j u_i\right)$. Material properties are provided by the blood's density ρ and viscosity μ, which are assumed constant for the present formulation, such that $\rho = 1050\,[\mathrm{kg/m^3}]$ and $\mu = 3.45\times10^{-3}\,[\mathrm{kg/m/s}]$.

Whilst it is recognised that blood viscosity is non-Newtonian (i. e. having a strain-rate dependence), its equivalent Newtonian approximation may be acceptable for arteries with diameters significantly larger than that of an erythrocyte $\sim 8\times10^{-6}$ [m] (Ambrosi *et al.*, 2012). The RCA geometry of figure 1 is sufficiently large to satisfy this condition and since

multiple periods of oscillation are to be computed in this study, the Newtonian approximation is used so that computational needs are reduced. However, it is recommended that in general, a high fidelity model of blood flow within coronary arteries should use a non-Newtonian viscosity formulation; see for example the models presented in Cho and Kensey (1991). It is also noted that the near-wall computational elements (required to resolve the mass transport boundary layer) are smaller than the diameter of an erythrocyte and hence, should resolve greater detail than the continuum description of blood would allow. Such flow detail is beyond the scope of the present study and may necessitate local corrections to the material properties of the blood fluid if required. This has been addressed in studies such as Huang *et al.* (2009), which have resolved such detail as the Fahraeus–Lindqvist effect (migration of erythrocytes away from the wall) and resulting variations in blood rheology.

Species transport

As with the flow, the distribution of blood-borne species is modelled as a continuum. That is, rather than tracking individual particles, their concentration is resolved on an Eulerian framework. For this study, the species of interest is low density lipoprotein (LDL); a single particle has a diameter of approximately 2.0×10^{-8} [m] (Teerlink *et al.*, 2004), which is about 10^5 times smaller than the internal diameter of a coronary artery. Thus, with such large difference between their respective diameters, the continuum description is expected to satisfactorily hold for the transport of LDL.
The presence of LDL is assumed to have no influence on the flow field. Therefore, LDL concentration transport is modelled as a passive scalar c that is advected with the flow (one-way coupling). The governing transport equation can be expressed in conservative form as

$$\partial_t c + \partial_i\left(u_i c - D\,\partial_i c\right) \;=\; 0\,, \tag{3}$$

where D is the isotropic diffusion coefficient, which for LDL is about $5.0\times10^{-12}\,\left[\mathrm{m}^2/\mathrm{s}\right]$ (Stangeby and Ethier, 2002). For the present case, c is a normalised concentration which has been scaled by its inflow value, such that $c = \mathrm{C}/\mathrm{C}_0$, where C is the concentration and C_0 is its inflow boundary value.

Boundary conditions

For a boundary Γ enclosing the volumetric flow space Ω_F, its inward-pointing surface normal is designated by $\boldsymbol{n}^+$ and outward-pointing surface normal by $\boldsymbol{n}^-$. The boundary conditions described here are for pulsatile flow conditions. Under steady-state conditions (i. e. when $\partial_t u_i = 0$ and $\partial_t c = 0$ in equations 2 and 3 respectively), the boundary conditions take their period-average values. At the inflow boundary Γ_I, a pulsatile Poiseuille flow profile of the form

$$u_i(\boldsymbol{x},t) \;=\; 2\,u_0(t)\left(1-\left(\frac{\|\boldsymbol{x}-\boldsymbol{x_c}\|}{\frac{1}{2}d_\mathrm{I}}\right)^2\right)n_i^+ \tag{4}$$

is assigned, where u_0 is the boundary-average velocity, which follows the time-periodic waveform defined in figure 2 and has period-average $\overline{u}_0$. The characteristic parabolic profile of the Poiseuille flow has its maximum at the boundary centroid $\boldsymbol{x_c}$, where $\boldsymbol{x}$ is a spatial coordinate on the boundary. To gauge-fix the pressure field, an arbitrarily selected Dirichlet condition $p = 0$ is assigned to the outflow boundary Γ_O; the precise value is not important under the present conditions. For the wall boundary Γ_W, a no-slip wall condition is assigned, such that $u_i = 0$.

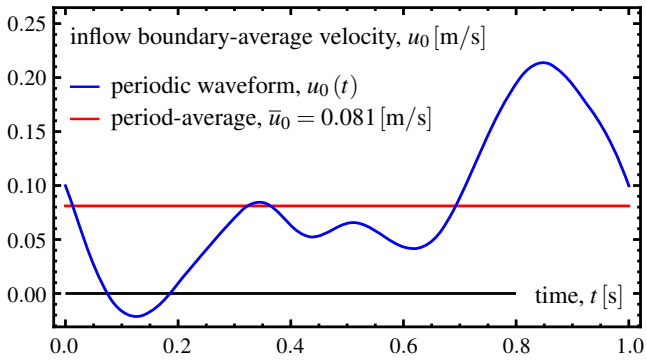

Figure 2: Plot of the RCA inflow waveform and its period-average; using an 8-term truncated Fourier series representation of the waveform provided in (Johnston *et al.*, 2006).

Since the LDL concentration field has been normalised by its inflow value, the inflow boundary Γ_I is therefore ascribed with the uniform condition $c = 1$. At the outflow boundary Γ_O, a zero flux condition $(\partial_i c)\,n_i^- = 0$ is assigned. Both these conditions are whole-boundary approximations and locally misrepresent the near wall LDL concentration due to the presence of a spatially growing boundary layer. However, due to the high Péclet number of LDL, its species transport equation is weakly elliptic, and so with the added flow-extensions, the effect of the misrepresented boundary conditions is not significant within the domain of interest. On the wall boundary Γ_W, the flux equilibrium condition

$$(u_i c - D\partial_i c)\,n_i^- \;=\; J_c \tag{5}$$

is ascribed, which describes the balance between advective flux into the wall and diffusive flux away from it. The net influx J_c of LDL into the arterial wall is set to be zero for the present conditions. The advecting velocity into the wall is set to be constant and equivalent to the water filtration velocity $J_u = 4.0\times10^{-8}\,[\mathrm{m/s}]$ (Stangeby and Ethier, 2002), such that $u_i n_i^- = J_u$. Note that this boundary condition has only been enforced in the species transport and has been omitted from the flow equations for this study. A more appropriate boundary condition for the flow equations should therefore correct the no-slip wall condition, such that

$$u_i n_i^- \;=\; J_u \tag{6}$$

$$u_i - (u_j n_j^-)n_i^- \;=\; 0\,. \tag{7}$$

The effect of the misrepresented boundary condition is not expected to influence the flow field significantly, because J_u is much smaller than $\overline{u}_0$ and the domain Ω_F is small; see the analytical solution for a straight artery with a semi-permeable wall in Wada and Karino (2000) for the influence of J_u.

Oscillatory flow data processing

An arbitrary scalar field variable φ that is transported within an oscillating flow of period-length T_p is considered. To compare the oscillating field variable with its steady-state, it is first necessary to decompose it into a time-invariant state. This is achieved with Reynolds periodic-decomposition, which decomposes the field variable into its period-average $\overline{\varphi}$ and time-dependent perturbation φ' components. Reynolds periodic-decomposition is defined

$$\varphi(t) \;=\; \left\{\overline{\varphi}+\varphi'(t)\;\middle|\;\overline{\varphi} \;=\; \frac{1}{T}\int_T \varphi(t)\,\mathrm{d}t,\;\; t\in T\right\}, \tag{8}$$

where $T = kT_p$ is the integration time and $k \geq 1$ is an integer multiplier. Under laminar flow conditions, the flow field is periodic at all relevant length scales; therefore, the decomposition may be made over a single period of oscillation ($k = 1$). However, under turbulent flow conditions, a sufficiently large number of periods ($k >> 1$) would be required for $\overline{\varphi}$ to become temporally invariant.

Applying the Reynolds periodic-decomposition to the flow (equations 1 and 2) and species transport (equation 3), and period-averaging, respectively yields

$$\partial_t \overline{u}_i = 0 \tag{9}$$

$$\rho \partial_t \overline{u}_i + \partial_j \left(\rho \left(\overline{u}_i \overline{u}_j + \overline{u'_i u'_j} \right) - \overline{\tau}_{ij} + \overline{p} \delta_{ij} \right) = 0 \tag{10}$$

$$\partial_t \overline{c} + \partial_i \left(\overline{u}_i \overline{c} + \overline{u'_i c'} - D \partial_i \overline{c} \right) = 0 . \tag{11}$$

It is noted that the period-averaged flow and mass equations are similar to their original form, except for the presence of added terms, which have emerged from the non-linear advective components of the equations. These added terms describe the period-aggregate influence of fluctuations about the period-average of their respective field variable. For the flow (equation 10) and species (equation 11), these added terms are respectively referred as the oscillatory advective-stress and oscillatory advective-flux.

Due to the presence of the oscillatory advective-stress and oscillatory advective-flux in the flow and species transport equations respectively, variations may emerge between the period-average and equivalent steady-state of their respective field variables. These variations may be subtle and difficult to qualitatively differentiate. A quantitative measure is therefore required, and is provided with the Steady Representation Index (SRI), which is defined

$$\mathrm{SRI}\{\varphi\} = \frac{\varphi|_{\mathrm{ss}} - \overline{\varphi}|_{\mathrm{ps}}}{\varphi|_{\mathrm{ss}} + \overline{\varphi}|_{\mathrm{ps}}} . \tag{12}$$

This index quantifies variations in a generic field variable φ that arise due to flow pulsatility, relative to its equivalent steady-state. The SRI is signed and bounded by the range $-1 \leq \mathrm{SRI} \leq 1$, such that a positive value $\mathrm{SRI}\{\varphi\}$ denotes that the steady-state value locally overestimates the field variable φ, and a negative value if it underestimates; at $\mathrm{SRI}\{\varphi\} = 0$, both steady and pulsatile conditions are locally equivalent.

For the flow field, oscillatory fluctuations have generally been measured via the Oscillatory Shear Index (OSI), which was designed to measure fluctuations in the wall shear stress $\boldsymbol{\tau_w}$ (He and Ku, 1996). In a previous study by the authors (Gabriel *et al.*, 2016), the Oscillatory Shear Index was generalised to the Oscillatory Flow Index (OFI), which extended the domain space of the index onto the flow-field, where

$$\mathrm{OFI} = \begin{cases} 1 - \dfrac{\|\overline{\boldsymbol{u}}\|}{\overline{\|\boldsymbol{u}\|}} & \text{on} \quad \Omega_{\mathrm{F}} \cup \partial\Omega_{\mathrm{F}} \setminus \Gamma_{\mathrm{W}} \\ \\ 1 - \dfrac{\|\overline{\boldsymbol{\tau_w}}\|}{\overline{\|\boldsymbol{\tau_w}\|}} & \text{on} \quad \Gamma_{\mathrm{W}} . \end{cases} \tag{13}$$

Note that the OSI is generally scaled to have a maximum value of 0.5; the scaling multiplier is removed in the above definition as it presents no added value. In the same study (Gabriel *et al.*, 2016), the Oscillatory Kinetic Energy Index (OKEI) was also introduced to measure the significance of the oscillatory fluctuations; by measures the trace (i. e. energy) of the oscillatory advective-stress tensor relative to that of the period-average flow. The OKEI was also extended to flow and wall spaces, and is defined

$$\mathrm{OKEI} = \begin{cases} \dfrac{\overline{\boldsymbol{u}' \cdot \boldsymbol{u}'}}{\overline{\boldsymbol{u}} \cdot \overline{\boldsymbol{u}} + \overline{\boldsymbol{u}' \cdot \boldsymbol{u}'}} & \text{on} \quad \Omega_{\mathrm{F}} \cup \partial\Omega_{\mathrm{F}} \setminus \Gamma_{\mathrm{W}} \\ \\ \dfrac{\overline{\boldsymbol{\tau}'_w \cdot \boldsymbol{\tau}'_w}}{\overline{\boldsymbol{\tau}_w} \cdot \overline{\boldsymbol{\tau}_w} + \overline{\boldsymbol{\tau}'_w \cdot \boldsymbol{\tau}'_w}} & \text{on} \quad \Gamma_{\mathrm{W}} . \end{cases} \tag{14}$$

By applying the OFI to the OKEI, direction-reversing (DR) and non direction-reversing (NDR) oscillations can be segregated and their significance measured, such that

$$\mathrm{OKEI}_{\mathrm{DR}} = \mathrm{OKEI} \times \mathrm{OFI} \tag{15}$$

$$\mathrm{OKEI}_{\mathrm{NDR}} = \mathrm{OKEI} \times (1 - \mathrm{OFI}) . \tag{16}$$

It is noted that a similar period-averaging technique was applied by Hong *et al.* (2012) to derive the period-average species concentration equations for LDL transport within the arterial wall. In that study, the authors argued that within the arterial wall, the period-averaged LDL concentration is significantly larger than its oscillatory perturbations and can thus be represented satisfactorily by the steady-state equivalent. In the present analysis, the period-averaged species equations within the lumen are demonstrated to inherit the period-aggregated influence of oscillatory perturbations via the oscillatory advective-flux term, which depending on its magnitude, can spatially modify the period-average species concentration from its steady-state equivalent. Therefore, in the same manner as the OKEI for the flow, the Oscillatory Species Advective-Flux Index (OSAFI) is proposed to measure the significance of the oscillatory advective-stress term in equation 11; the OSAFI is defined

$$\mathrm{OSAFI} = \frac{\|\overline{\boldsymbol{u}' c'}\|}{\|\overline{\boldsymbol{u}}\ \overline{c}\| + \|\overline{\boldsymbol{u}' c'}\|} \quad \text{on} \quad \Omega_{\mathrm{F}} \cup \partial\Omega_{\mathrm{F}} \setminus \Gamma_{\mathrm{W}} . \tag{17}$$

Computational implementation

The system of flow and species transport equations was implemented into the cell-centred finite-volume solver ANSYS Fluent v17.2, with in-house user-defined functions for customisation of the solver and data-processing. Computations were made with double-precision on a 64-bit serial machine. For the flow equations, pressure-velocity coupling was attained via the SIMPLE algorithm. Flow variable discretisation was made using a second-order upwind scheme and pressure discretisation using the *standard* ANSYS Fluent scheme (a neighbour-cell interpolation method using momentum equation coefficient weighting). For species (LDL concentration) discretisation, a first-order upwind scheme was used; this scheme was implemented to avoid numerical instabilities arising due to the high Péclet number associated with the species transport. Temporal discretisation of all equations was made with an implicit first-order forward-differencing scheme. Field variable gradients were derived using least-squares cell-based interpolation.

RESULTS AND DISCUSSION

For the pulsatile flow (i. e. temporal) case, computations were terminated at the end of the 20th period of oscillation. It was found that from zero initial conditions, the flow field had converged to a steady-periodic state by the fourth period (i. e. the period-average remained unchanged with successive periods). However, as expected of the high Péclet number associated with LDL transport, the LDL concentration field

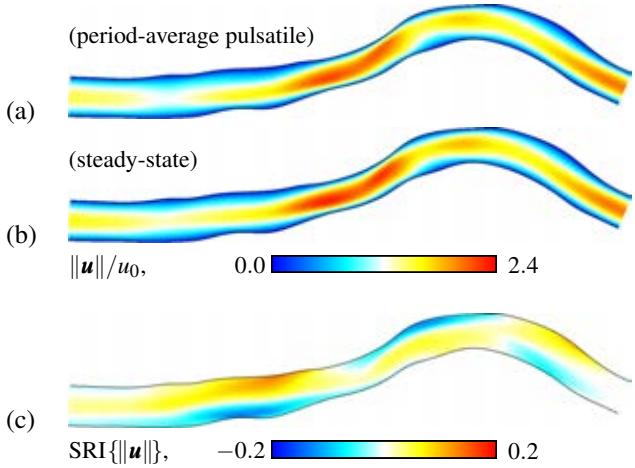

Figure 3: Plot of normalised velocity magnitude on a longitudinal mid-cut of the artery; for (a) period-average of pulsatile flow, (b) steady-state flow and (c) Steady Representation Index of both conditions.

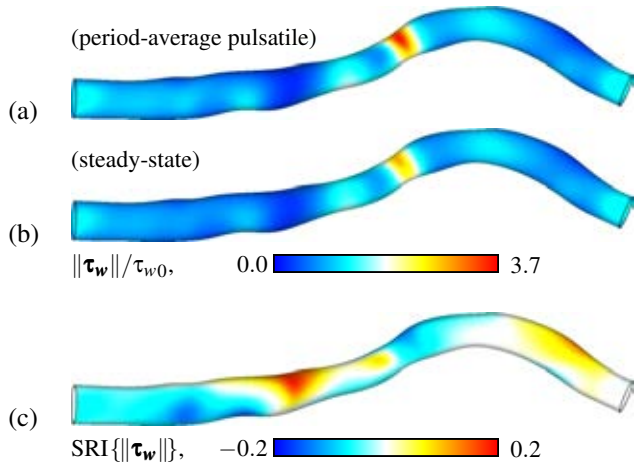

Figure 4: Plot of normalised wall shear stress magnitude on the wall; for (a) period-average of pulsatile flow, (b) steady-state flow and (c) Steady Representation Index of both conditions, where $\tau_{w0} = 8\mu u_0/d_I$ is the inflow's equivalent Poiseuille wall shear stress.

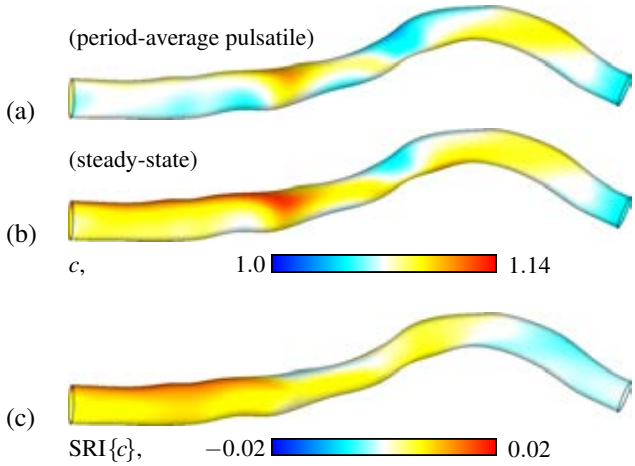

Figure 5: Plot of normalised LDL concentration on the wall; for (a) period-average of pulsatile flow, (b) steady-state flow and (c) Steady Representation Index of both conditions.

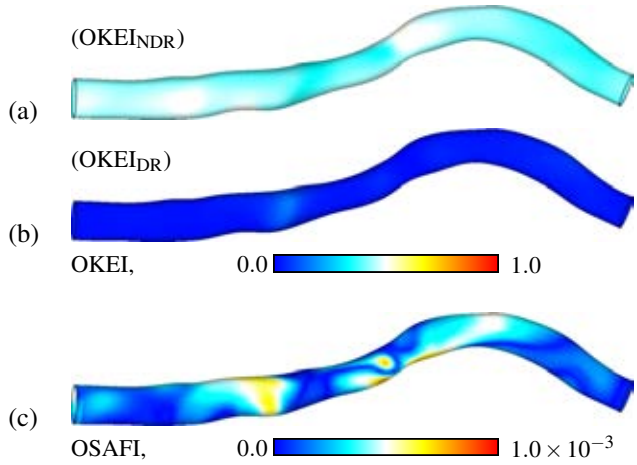

Figure 6: Plot of OKEI on the wall; for (a) NDR and (b) DR oscillations. Also, a plot of (c) OSAFI on a near-wall surface within Ω_F (i. e. taking measurements at the first element layer from the wall).

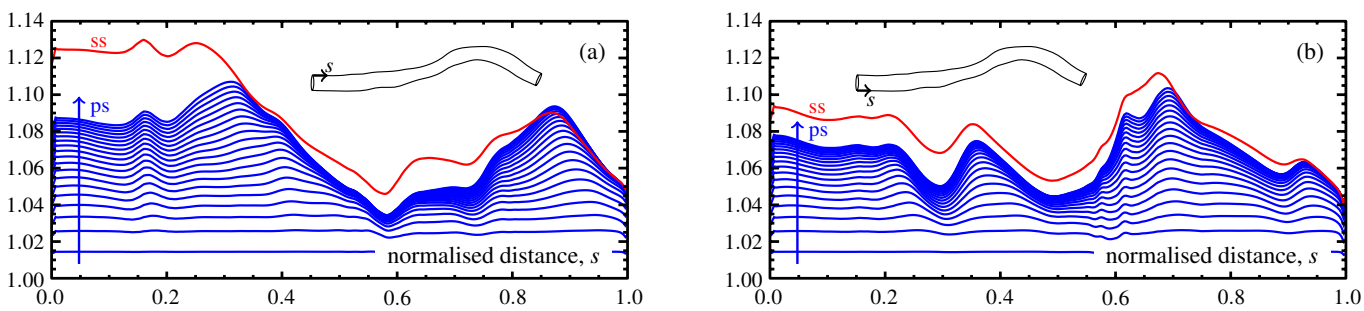

Figure 7: Plot of normalised LDL concentration along the normalised distance of the (a) upper and (b) lower span of the RCA; comparing period-averaged pulsatile-state (ps) and equivalent steady-state (ss) conditions. The direction of the arrow is from period 1–20.

was yet to converge onto a steady-periodic state from initial conditions $c = 1$ (see figure 7). Nevertheless, to give preliminary insight into what is expected of a converged periodic state for the LDL concentration field, the 20th period results are investigated for the present study.

Observation of the flow and wall shear stress distributions in figures 3 and 4 respectively, reveals that the period-average of the pulsatile flow displays similar characteristic to that of its equivalent steady-state condition. However, subtle variations can be observed, particularly in the magnitude of the velocity and wall shear stress at the narrowing of the artery (near its longitudinal centre) and at the expansion thereafter

(just before the outflow). This is confirmed by the SRI for these respective indices, which also reveals that its sign is not homogeneous but a seemingly even distribution of positive and negative; indicating that the period-average of the pulsatile flow is both overestimated and underestimated relatively evenly by its steady-state equivalent.

For the LDL concentration (figure 5), it is noted that the period-average distribution for the 20th period is significantly far from converged, and many more periods are required before a steady-periodic state is achieved. When compared to the steady-state case, it appears that both distributions resemble each other (since regions of high and low concentrations seem to spatially coincide), though their respective magnitudes substantially differ. Correspondingly, it is expected that the steady-periodic state may also behave similarly to the 20th period. From the corresponding signed SRI distribution, it is noted that the period-average of the oscillatory concentration field is mostly less than that of its steady-state equivalent. Observation of successive period-averaged concentration profiles along the span of the artery (figure 7) reveals that the concentration field is currently incrementally increasing in magnitude away from its initial condition $c = 1$. This behaviour appears to be monotonic and slowing down with each successive period, indicating that the steady-periodic state is a converging limit.

It is difficult to ascertain the influence of flow oscillations on the flow and species field variables, from their respective distributions alone. However, this information can be determined from their corresponding oscillatory indices. From figure 6, it can be observed that the OKEI is significant throughout the artery, with NDR oscillations dominating. A small distribution of $\mathrm{OKEI}_{\mathrm{DR}}$ is also observed, though this is insignificant relative to that of the $\mathrm{OKEI}_{\mathrm{NDR}}$. The magnitude of these distributions is generally equal to or less than 0.5, indicating that the oscillatory advective-stress is not dominant though moderately influential in modifying the period-average flow field from its equivalent steady-state.

For the OSAFI, a more diverse distribution is observed, where there seems to be little correlation with that of the OKEI. However, a similar distribution is observed with the $\mathrm{SRI}\{\|\boldsymbol{\tau}_{\boldsymbol{w}}\|\}$ (figure 4), indicating a possible relation with the gradient of the flow velocity. Though, further analysis is required before this can be ascertained.

CONCLUSION

The oscillatory transport of pulsatile blood flow and blood-borne species (low density lipoprotein) has been investigated in the present study. It was determined from their respective period-averaged transport equations that oscillatory influence is inherent to the period-average transport. This influence is prominent in the advective terms of the equations and manifests as the period-aggregate of oscillatory advective-stresses and advective-fluxes within the flow and species transport respectively. These terms are identified to be the cause for parting the period-average transport from its equivalent steady-state condition. To investigate these terms, pulsatile blood flow within a human right coronary artery is investigated and oscillatory indices developed to measure their significance. It was observed that though a direct correlation could not be ascertained between the oscillatory indices for flow and species transport respectively, there was sufficient similarity to imply a potential relationship. It is the objective of this study that such a relationship can be determined and modelled, so as to better resolve pulsatile species transport without explicitly resolving all periods of oscillation.

ACKNOWLEDGEMENTS

This work was supported by an Australian Government Research Training Program Scholarship and a grant from the CSIRO through the ATN Industry Doctoral Training Centre. The Biofluid Mechanics Lab, Charité Universitätsmedizin Berlin is acknowledged for providing the RCA geometry.

REFERENCES

AMBROSI, D., QUARTERONI, A. and ROZZA, G. (eds.) (2012). *Modeling of Physiological Flows*, vol. 5 of *Modeling, Simulation & Applications*. Springer Milan, Milano.

CHO, Y.I. and KENSEY, K.R. (1991). "Effects of the non-Newtonian viscosity of blood on flows in a diseased arterial vessel. Part 1: Steady flows." *Biorheology*, **28(3-4)**, 241–62.

GABRIEL, S.A., DING, Y. and FENG, Y. (2016). "Extending the Oscillatory Index to discern oscillatory flow modes". *20th Australasian Fluid Mechanics Conference*, 1–4. Australasian Fluid Mechanics Society, Perth, Australia.

HE, X. and KU, D.N. (1996). "Pulsatile flow in the human left coronary artery bifurcation: average conditions." *Journal of Biomechanical Engineering*, **118(1)**, 74–82.

HONG, J., FU, C., LIN, H. and TAN, W. (2012). "Non-Newtonian effects on low-density lipoprotein transport in the arterial wall". *Journal of Non-Newtonian Fluid Mechanics*, **189-190**, 1–7.

HUANG, J., LYCZKOWSKI, R.W. and GIDASPOW, D. (2009). "Pulsatile flow in a coronary artery using multiphase kinetic theory". *Journal of biomechanics*, **42(6)**, 743–54.

JOHNSTON, B.M., JOHNSTON, P.R., CORNEY, S. and KILPATRICK, D. (2006). "Non-Newtonian blood flow in human right coronary arteries: transient simulations." *Journal of biomechanics*, **39(6)**, 1116–28.

LIU, X., FAN, Y., DENG, X. and ZHAN, F. (2011). "Effect of non-Newtonian and pulsatile blood flow on mass transport in the human aorta". *Journal of Biomechanics*, **44(6)**, 1123–1131.

SAKELLARIOS, A.I. *et al.* (2013). "Patient-specific computational modeling of subendothelial LDL accumulation in a stenosed right coronary artery: effect of hemodynamic and biological factors." *American journal of physiology. Heart and circulatory physiology*, **304(11)**, H1455–70.

STANGEBY, D.K. and ETHIER, C.R. (2002). "Computational analysis of coupled blood-wall arterial LDL transport". *Journal of biomechanical engineering*, **124(1)**, 1–8.

SUN, N. *et al.* (2007). "Influence of pulsatile flow on LDL transport in the arterial wall". *Annals of biomedical engineering*, **35(10)**, 1782–90.

TARBELL, J.M. (2003). "Mass transport in arteries and the localization of atherosclerosis". *Annual review of biomedical engineering*, **5(1)**, 79–118.

TEERLINK, T., SCHEFFER, P.G., BAKKER, S.J.L. and HEINE, R.J. (2004). "Combined data from LDL composition and size measurement are compatible with a discoid particle shape". *Journal of lipid research*, **45(5)**, 954–66.

THIRIET, M. (2008). *Biology and Mechanics of Blood Flows. Part II: Mechanics and Medical Aspects*. Springer, New York, NY.

WADA, S. and KARINO, T. (2000). "Computational Study on LDL Transfer from Flowing Blood to Arterial Walls". T. Yamaguchi (ed.), *Clinical Application of Computational Mechanics to the Cardiovascular System*, 157–173. Springer Japan, Tokyo.